01,14

Molecular dynamics study of mechanical properties of crystalline and amorphous nickel nanoparticles

© G.M. Poletaev[1], V.V. Kovalenko[2]

[1] Polzunov Altai State Technical University,
Barnaul, Russia
[2] Siberian State Industrial University,
Novokuznetsk, Russia

E-mail: gmpoletaev@mail.ru

Received May 14, 2025
Revised June 22, 2025
Accepted July 30, 2025

The molecular dynamics method was used to study the compression deformation of nickel nanoparticles with crystalline and amorphous structures. It was shown that the strength of the nanoparticles increases with increasing deformation rate, and decreases with increasing temperature. Anisotropy of mechanical properties occurs during deformation of single-crystal nanoparticles. In particular, the compressive strength along the [111] and [110] directions was found to be approximately 30−40 % greater than the compressive strength along the [112] direction. As the size of the nanoparticles, both single-crystal and amorphous, decreased, their strength increased, and the value of deformation at which the maximum stress was achieved also increased. One of the possible reasons for the influence of particle size on its strength in the case of an amorphous structure may be compaction and partial crystallization of the structure near the points of load application.

Keywords: molecular dynamics, nanoparticle, compression, deformation, amorphous structure.

DOI: 10.61011/PSS.2025.08.62249.119-25

1. Introduction

A lot of attention has been paid in recent decades to metal nanoparticles due to their unique physical, chemical and optical properties, which are caused by a high portion of the free surface, quantum-mechanical and topological effects [1]. The nanoparticles are promising for use in such fields as microelectronics, optoelectronics and plasmonics [2,3], medicine and biology [4,5], chemical catalysis, production of gas sensors [6,7]. In addition to other unique properties of the nanoparticles, their mechanical properties are also very promising in terms of practice and they are often much better than properties of respective bulk materials. Special experimental studies that are usually carried out with using nanoindenting methods [8,9] made it possible to identify a number of key specific features. Thus, it was found out that the nanoparticles can be much stronger than the bulk materials. The strength of the single-crystal particles can reach gigantic values — up to several tens of GPa [10–20]. For example, when compressing single-crystal nickel nanoparticles of the diameter of 210 nm in the experimental study [13] by nanoindenting, the strength of 34 GPa was recorded [13]. The unique mechanical properties of the nanoparticles are already used now, for example, when designing nanocomposite materials, in which the metal nanoparticles act as fillers for improving tribological properties of lubricants [21–24].

It was obtained in some studies performed both by means of direct nanoparticle-compression experiments as well as by means of respective computer simulation that with decrease of a particle size their strength increased [13,16–20]. Presently, some researchers believe that this effect is related to reduction of an available volume for operation of a dislocation source when the size of the single-crystal particle decreases [25–28], i. e. it is assumed that the influence of the particle size on its strength is a specific feature of crystalline particles. However, the data of the studies that included simulation of compression of non-crystalline particles differ: in some studies, the particle size the particle size within an error had almost no impact on the strength [29,30], whereas it nevertheless occurred in the others [31]. The authors assumed in the study [31] that it was possible to observe increase of strength of small non-crystalline particles due to formation of a denser structure in compression locations.

Another interesting observation concerning deformation of the nanoparticles is increase of fracture toughness when the nanoparticle size is decreased [32]. It was found by means of high-resolution transmission electron microscopy that silver nanoparticles of the size below 10 nm can be deformed similar to liquid drops at the room temperature [33]. In the study [13], with nanoindenting of the nickel particles, the maximum compression strength was achieved at deformation 10−20 %. It was shown in the studies [34–36] that quite small particles that are made of fragile materials such as silicon or magnesium oxide could also be plastically deformed.

Available experimental results for the mechanical properties of the nanoparticles were mainly obtained by compression and indenting, which is the only simple loading

mode that can be applied to the nanoparticles. In this case, computer simulation at an atomic level is an effective complement. The present study is aimed at comparing the mechanical properties of round nickel nanoparticles with a crystalline and an amorphous structure in compression deformation by means of molecular dynamics simulation. Presently, the nanoparticles with the amorphous structure are of large interest [37–39]. Atoms in the amorphous particles are in a non-equilibrium state and have a higher Gibbs energy as compared to atoms in a crystal and have a unique electron structure, thereby making them promising in the field of catalysis, biomedicine, optics and electronics [40–42]. The present study is mainly focused on studying the influence of the (crystalline or amorphous) structure of the nanoparticles and their size on their strength and fracture toughness. Besides, the study also deals with the influence of orientation of compression, a temperature and a deformation rate on the mechanical properties of the particles. It also includes consideration of specific features of a deformation progress in case of the single-crystal and amorphous nanoparticles. The nickel particles are selected as an example due to their wide practical application. Nickel has high corrosion resistance, higher plasticity and ductility, and it is a good catalyst. Additionally, for the single-crystal nickel nanoparticles, there are data of experimental strength studies [13] as well as results of simulation by other authors [20,43].

2. Model description

Interactions of the nickel atoms with each other in the molecular dynamics model were described by means of an embedded atom method potential (EAM) from the study [44], which was created with taking into account experimental data and results of *ab initio* calculations of the various nickel properties. This potential has proven itself when performing various molecular dynamics studies and was successively tested within a wide range of the mechanical and structure and energy properties, including processes of plastic deformation, structure and phase transformations, self-diffusion [44–49]. We previously used it when investigating melting and crystallization of the nickel nanoparticles [48,49].

The round metal particle in the model at the first stage was created by cutting a ball of the respective size out of the perfect nickel crystal. The particles of the diameter from 1.5 to 20 nm were considered. Free space was simulated around the particle. I. e., a canonical NPT-ensemble was used (the number of the atoms N, the pressure P and the temperature T remain constant during simulation). A Nose–Hoover thermostat was used to monitor constancy of the temperature. The step of time integration in the molecular dynamics method was 2 fs.

It is known that for quite small nanoparticles that include at most 1000–1500 atoms (the diameter is less than about 2.7–3.2 nm for nickel) the face-centered cubic

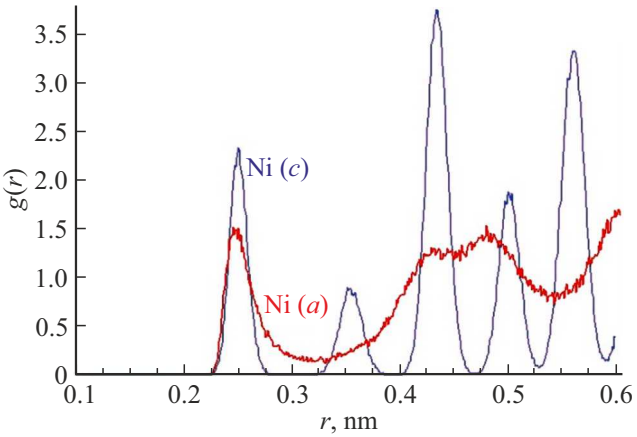


Figure 1. Functions of the radial atom distribution for the crystalline (c) and the amorphous (a) nickel nanoparticle at the temperature of 200 K.

(FCC) structure is not energetically favorable and competes with, for example, icosahedral and decahedral structures, especially in case of arbitrary (not „optimal“ c in terms of the energy of the atoms in the particle) cutting of the ball from the initial FCC crystal [50,51]. In the present study, when investigating deformation of the single-crystal nanoparticles, all the particles had the FCC initial structure.

After the initial crystalline round particle was created, structural relaxation was carried out at the constant temperature of 500 K for 20 ps, and an equilibrium state of the atom structure was established for the pre-defined temperature. After relaxation, the particles were cooled to the minimum possible temperature close to 0 K.

The amorphous-structure particles were created by superfast (at the rate of about 10^{16} K/s) cooling of the particles that were melt when being heated to the temperature which significantly exceeded the melting point (usually, 2000–2500 K). When the metal is cooled with such a rate, homogeneous crystallization does not have time to occur and the amorphous structure that is typical for a supercooled liquid is formed [52]. The stage of superfast cooling was followed by structural relaxation at the temperature of 200 K for 50 ps, thereby resulting in rebuilding of the structure and forming a metastable structure that was resistant to structural transformation up to a devitrification temperature. A quality of the amorphous structure was checked by means of diagrams of radial atom distribution and by an average energy of the atoms in the nanoparticles. Figure 1 shows graphs of the radial distribution functions for the crystalline and amorphous nickel nanoparticle. One of the signs of the amorphous state is no peak on the distributions around the second coordination sphere of the FCC lattice. After relaxation, the particles were cooled to the minimum possible temperature close to 0 K.

The nanoparticle was compressed in the model by moving virtual planes at both sides of the particles at the constant rate (Figure 2). Interaction of the atoms with virtual bound-

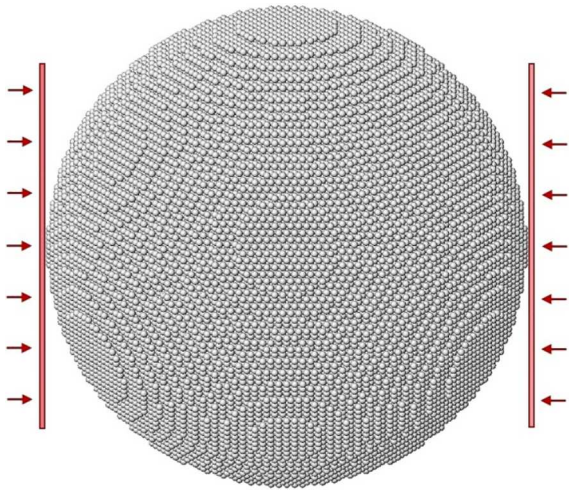


Figure 2. Diagram of simulation of compression of the nickel nanoparticle.

aries was pre-defined as absolutely elastic one. This method was used in the most of the studies dedicated to molecular dynamics simulation of nanoparticle compression. At this, the rate of movement of the flat boundaries is usually pre-defined within the range from 10 to 50 m/s [14,15,18,19], while the initial temperature is usually pre-defined as low as possible — near 0 K. However, it is known that the temperature of deformation and the deformation rate, especially within a range of relatively high values, affect the mechanical characteristics [53]. Consequently, in the present study, we additionally investigated the influence of the compression rate on them.

A compressive stress was determined as a ratio of the resultant force that acts on the virtual flat boundaries from the atoms to a total area of a contact spot. The area of the contact spot was calculated as a number of the atoms at the boundary, which is multiplied by an average area per one atom.

3. Results and discussion

Figure 3 exemplifies the stress-deformation dependences when compressing the single-crystal nickel particles of the diameter of 10 nm at the rate of 10 m/s along the directions [111], [110] and [112] (these are mutually perpendicular axes) at the initial temperature of 0 K. Specific features of these dependences may include presence of several local peaks that are related to structure tuning within the contact spot, where a load is applied. For this reason, an elastic region is often unpronounced — there are usually several local peaks to a maximum stress, which is defined in some studies as nanoparticle hardness [14–19]. The maximum stress values are very high and for the directions [111] and [110] they exceed 18 GPa in this case. A quite viscous, nonfragile nature of deformation of the particles can also be noted: the maximum stress values are observed at the very high deformation values of several percent, while it is almost 12 % for the direction [112].

As expected, a compression direction affects the mechanical characteristics for the single-crystal nanoparticle: when compressing along the directions [111] (perpendicular to the most closely-packed planes) and [110] (along the most closely-packed direction) the maximum stress was always noticeably larger than the stress achieved when compressing along [112]. It should be said that a qualitatively-similar result was also obtained in the study [14] when compressing the single-crystal copper particles (which also has the FCC lattice as in the case of nickel). The strength difference when compressing in the said directions is explained by a difference of a so-called reduced shift stress which is defined as a stress that induces the shift along the direction of propagation of dislocations in the FCC crystal, i. e. along the direction of the type $\langle 110 \rangle$ within a slip plane of the type $\{111\}$.

The influence of the deformation rate and the temperature on the mechanical characteristics is often underestimated during molecular dynamics simulation of nanoparticle compression. We have additionally studied this influence using the example of the single-crystal nickel nanoparticles of the diameter of 10 nm when compressing along the three directions — [111], [110] and [112]. Figure 4, *a* shows the dependences of strength of the particle $\sigma_{\max}$ on the compression rate. The rate varied from 2 to 500 m/s. The maximum rate value considered by us was just by an order of magnitude less than the speed of sound in nickel. As can be seen, increase of the deformation rate results in increase of the maximum stress of the particle, which can be achieved during compression. It is a known and experimentally-observed relationship that is explained by a finite speed of propagation of elastic waves and dislocations [53]. For the deformation rate of less than about

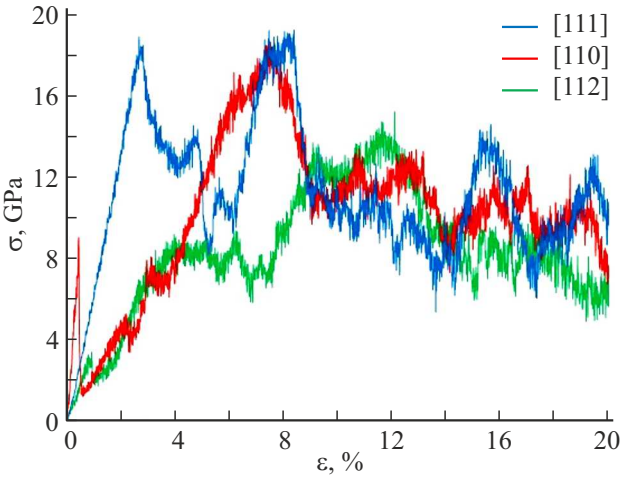


Figure 3. Stress-deformation dependences when compressing the single-crystal nickel particles of the diameter of 10 nm at the rate of 10 m/s along the directions [111], [110] and [112] at the initial temperature of 0 K.

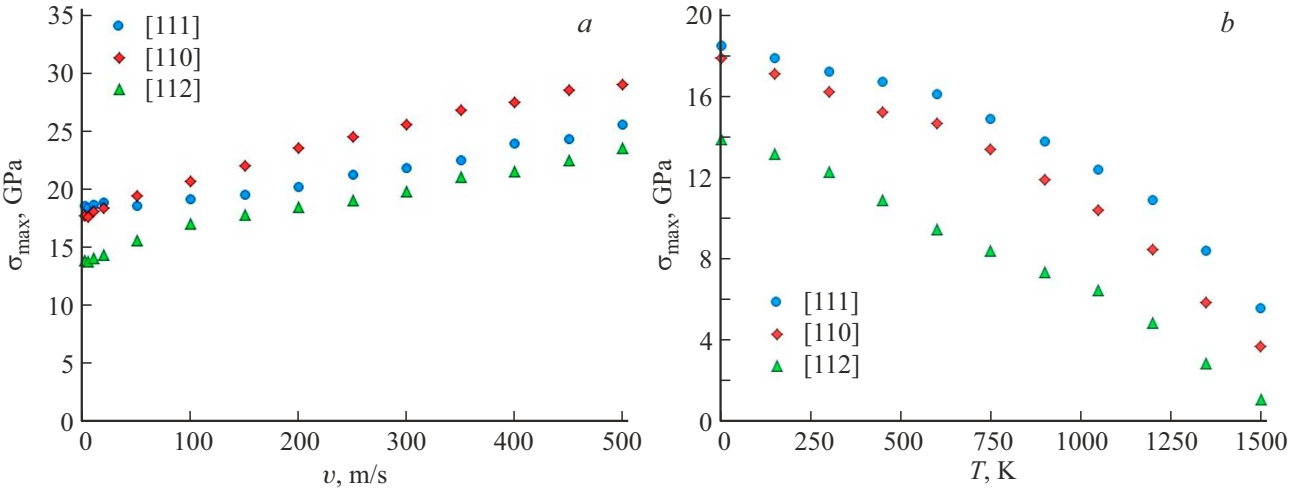


Figure 4. Dependences of strength of the single-crystal nanoparticle of the diameter of 10 nm: *a*) on the compression rate (at the initial temperature of 0 K); *b*) on the temperature (at the compression rate of 10 m/s).

10 m/s, its influence on the value of σ_{max} decreased and was not so obvious.

The temperature also significantly affects the mechanical characteristics: as known, with increase of the temperature the elastic moduli decrease, while plastic deformation and formation of dislocations occur at smaller values of deformation [53]. The same is also referred to deformation of nanoparticles. Figure 4, *b* shows the dependences of strength of the single-crystal particle of the diameter of 10 nm on the temperature. It is clear that with increase of the temperature the strength of the nanoparticle decreases.

When comparing the dependences of Figure 4, *a* and *b*, one interesting specific feature can be noted: when the deformation rate is less than about 100 m/s, the compressive strength along [111] is usually a little higher than that along along [110], but, on the contrary, at the rates above 100 m/s, the compressive strength along [110] becomes higher than for [111]. At the same time, with increase of the deformation rate the difference between the strength values for the directions [110] and [111] increases. It seems that at such high rates that are just by an order of magnitude less than the speed of sound, it is related to anisotropy of propagation of the elastic waves in the crystal. All further studies of nanoparticle compression were carried out at the deformation rate of 10 m/s and the initial temperature of 0 K.

Figure 5, *a* shows the dependences of the strength σ_{max} on the size of the single-crystal nanoparticle. First of all, it should be noted that as the particle size decreases, there is a tendency to strength increase, indeed, which has been already reported in other studies. In addition to the sizes, which are usually considered when simulating nanoparticle compression (about tens of nanometers), we have considered quite small particles of the diameter of up to 1.5 nm, in which plastic shears develop differently as compared to the large particles — as a rule, it is almost impossible to find dislocation in them inside the particle. However, as it is clear in Figure 5, *a*, the strength-growing tendency is preserved with decrease of the size.

With the particle diameter of less than about 8 nm, the Figure 5, *a* exhibits a noticeably large spread of the strength values as compared to the large-size particles. It is primarily due to errors of calculation of the stress in the model, which increased with decrease of the particle size both due to an error of determination of the area of the contact spot and due to increase of the influence of a particle form and a relief of its surface on the error in this case. Small deviations of the particle form from a ball shape or presence of atomic steps on the surface resulted in noticeable deviations of the obtained values.

As said above, the studies were performed for round single-crystal nanoparticles that were obtained in the model as a result of cutting the ball out of the initial FCC crystal. However, according to the studies [50,51], in terms of energy at the low temperatures the optimal particles are either icosahedrons at the small sizes or truncated FCC octahedrons at the quite large sizes. One should expect record strength values for such perfect particles, as, for example, in the studies [13,20], which have obtained the strength values about a half times higher than those obtained in our study, for such perfect single-crystal nickel particles. For example, by nanoindenting the single-crystal nickel particles which are shaped as the truncated octahedron, the study [13] has obtained the strength values from 10 GPa for the particles of the size of 880 nm to 34 GPa for the particles of the size of 210 nm. The study [20] that was carried out by means of simulation by the molecular dynamics method varied the strength of the nickel nanoparticles shaped as the truncated octahedron from 20 GPa for the particles of the diameter of 20 nm to 35 GPa for the particles of the diameter of 5 nm. However, during molecular dynamics simulation of compression of the ball-shaped

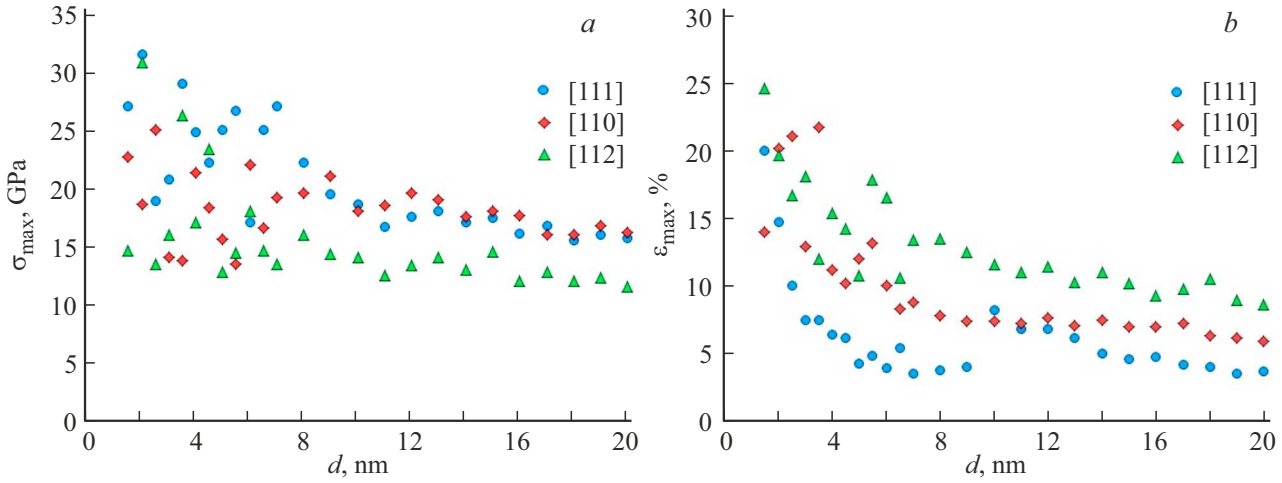


Figure 5. Dependences of *a*) the maximum stress and *b*) the respective deformation on the size of the single-crystal nanoparticle.

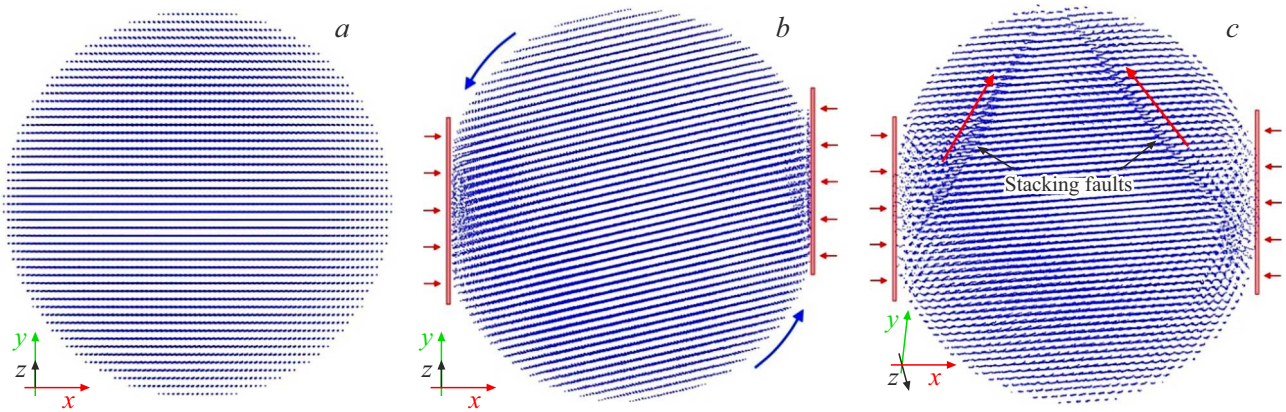


Figure 6. Main stages of plastic deformation of the single-crystal nanoparticles as exemplified by compression of the 10-nm particle: *a*) the initial structure of the particle; *b*) rotation of the particle (deformation is 9.20 %); *c*) formation of dislocations from the points of load application (deformation is 13.75 %).

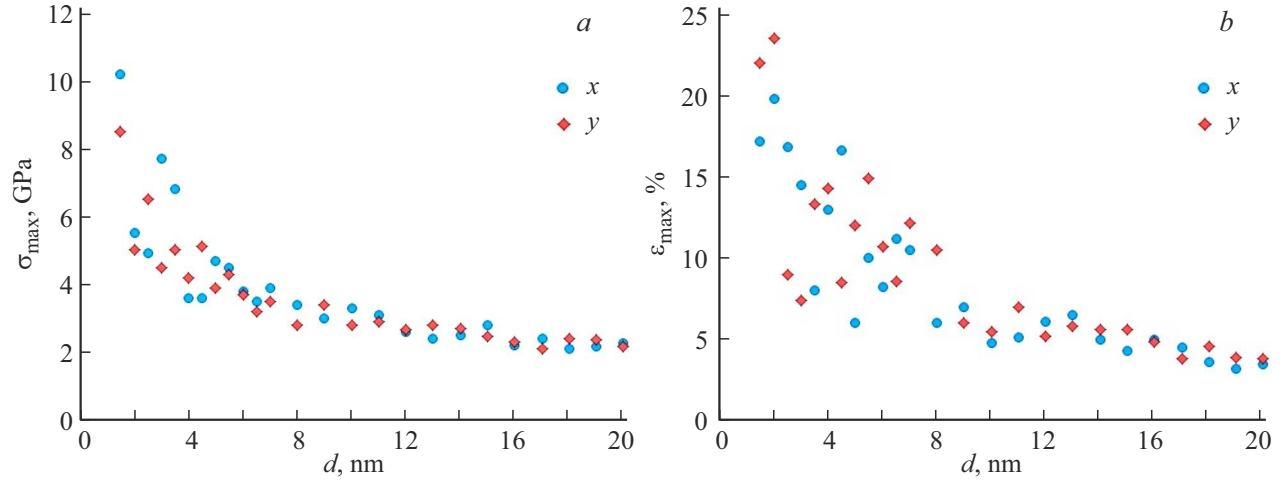


Figure 7. Dependences of *a*) the maximum stress and *b*) the respective deformation on the size of the amorphous nanoparticle.

nickel nanoparticle of the diameter of 10 nm, the study [43] had the much lower strength — 13.5 GPa.

Figure 5, *b* shows the dependences of the deformation values, at which there is the maximum stress ε_{max}, on the particle size. As the particle size decreases, the values of ε_{max} increase, which agrees to results of the studies of other authors [32–36]. In particular, in the experimental study [13], the maximum stress for the single-crystal nickel particles was achieved with deformation 10–20 %, while in the study [43] that was carried out by molecular dynamics simulation the maximum stress was achieved for the nickel nanoparticles of the diameter of 10 nm with compression for 5–15 %.

As can be seen in Figure 5, *b*, a stronger increase of the value of ε_{max} is observed with the particle sizes of less than about 8 nm. For the value of ε_{max} during compression of the single-crystal particle as well as for the strength, there is also anisotropy observed: the maximum values of the magnitude of ε_{max} were obtained when compressing the particles along the direction [112], so were the smallest ones for the direction [111].

Figure 6 shows images that illustrate the main stages of deformation of the nanoparticles during compression. The first stage included formation of the flat contact spots — regions of load application. The structure was „crushed" to a certain value of the contact area, which was followed by an interval of elastic deformation, after which the contact area was again increased, usually sharply, with stress drop (Figure 3) and it was temporarily fixed with a subsequent new interval of elastic deformation. The next stage, which set in usually before reaching the maximum value of the stress, was cooperative rotation of the entire structure of the particle, sometimes by a quite significant angle. As exemplified by Figure 6, *b*, the structure of the particle of the diameter of 10 nm is rotated around the axis of the type [112] by the angle of about 13°. It is noteworthy that as the particle size decreased, a portion of this stage, i. e. the rotation stage, increased, so did the angle by which the crystal structure was rotated. The rotation stage was followed by a stage of formation and propagation of dislocations that were usually formed from the contact spots, i. e. from the points of load application (Figure 6, *c*). Figure 6, *c* shows a moment of formation of two complexes made up of two partial dislocations with a stacking fault between them. In the illustrated example, some partial dislocations of these two pairs already almost get to the particle surface, while the two others are still near the contact spots. With further compression, these partial dislocations will be torn off to surface after the first ones. Formation of dislocations during compression of the nanoparticles was investigated, for example, in the studies [14,15,19].

When studying deformation of the nanoparticles with the amorphous structure, they were also provided with constructed dependences of the maximum stress and the respective deformation on the particle size, which are shown in Figure 7. Each amorphous particle was compressed along two different mutually perpendicular directions. As can be seen in Figure 7, *a*, despite assumptions of authors of the studies [25–28] that the influence of the size is a specific feature of crystalline particles only, we have obtained that the size affects the strength of the particles with the amorphous structure, too: as can be seen in Figure 7, *a*, as the size of the amorphous particles is reduced, the strength of the particles increased. At the same time, this influence was manifested more strongly for quite small particles of the diameter of less than about 8 nm. The strength of the amorphous particles was, as quite expected, in several times less than the strength of the single-crystal particles. Only for the quite small particles of the diameter of less than about 3 nm, it turned out to be curiously high and untypical for a „supercooled liquid".

Figure 7, *b* shows the dependence of the values of deformation that corresponds to the maximum stress, on the size of the amorphous particle. Here, we can again clearly see the influence of the particle size: as in the case of the crystalline nanoparticle, as its diameter decreases, the value of ε_{max} increases. It is interesting that the values of ε_{max} turned out to be even lower than for the single-crystal particles on average (Figure 5, *b*).

One of the possible reasons of the influence of the particle size on its strength in case of the amorphous structure may be probable compaction of the structure (which was already proposed by authors of the study [31]) and, respectively, its strengthening near the contact spots, i. e. locations that are most intensely compressed. When studying variation of the structure of the amorphous particles during compression, in most cases we really noticed an interesting phenomenon: at a certain stage, usually with deformation of more than 8–10 %, partial crystallization occurred near the contact spots — a crystalline structure was formed near the points of application of the maximum load. At the same time, the most closely-packed atomic planes of the type (111) were usually oriented parallel to a spot plane. Figure 8 exemplifies such partial crystallization near „islets" for the particles of the diameter of 10 and 12 nm.

Compaction of the structure and formation of the crystalline phase near the contact spots can affect an increase of the strength of the amorphous nanoparticles. However, the influence of the particle size on a portion of the crystalline phase at the start of its formation and on its growth rate during compression of the particle turned out to be ambiguous, especially for the quite small particles. It was noted that as the particle size was reduced, probability of formation of the crystalline phase decreased, which is apparently explained by the fact that with a small particle size its radius becomes close to a critical radius of a nucleus of the crystallite phase (i. e., to the radius of the growing crystallite phase, at which it becomes stable). At the same time, the small amorphous particles usually demonstrated anomalously high strength (Figure 8, *a*). It should be also noted that when there was still crystallization of the small amorphous particles, their final structure usually had less structural defects as compared to the structure

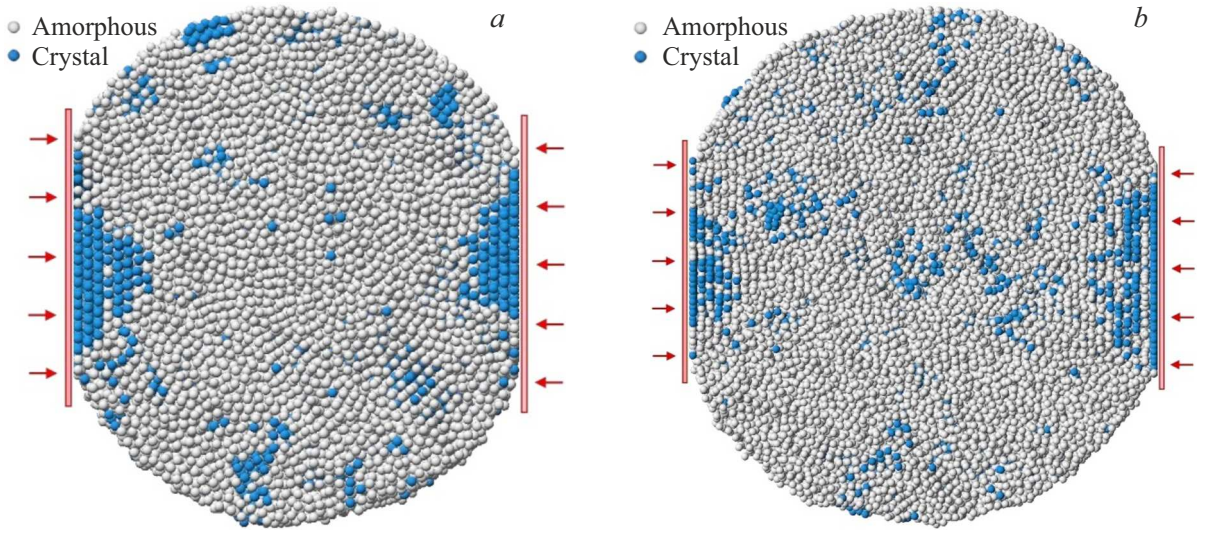


Figure 8. Partial crystallization near the points of load application during compression of the amorphous nanoparticles. Sections of the particles of the following diameter are shown: *a*) 10 nm (deformation is 12.13 %); *b*) 12 nm (deformation is 11.90 %).

of the large particles after their crystallization, as it took place, for example, when we studied crystallization of the nanoparticles during cooling from a molten state in the study [49].

Thus, it turns out that the influence of the particle size on its mechanical properties is complex and has a multifactorial nature. A volume required for forming and developing dislocations is important for the crystalline particles, while the amorphous particles necessitate compaction and strengthening, often in combination with partial crystallization, of the structure near the points of load application. Besides, it is interesting and important in this case to study factors that affect the area of the very contact spot, with taking into account that this area determines a value of the calculated stress.

4. Conclusion

The molecular dynamics method was used to study compression deformation of the nickel nanoparticles with the crystalline and the amorphous structure. We have studied the influence of the nanoparticle size on their strength and on the value of deformation, at which the maximum stress is achieved. We have also studied the influence of the deformation rate, the temperature and orientation of compression on the mechanical characteristics of the single-crystal nanoparticles. The following conclusions are made.

1. With increase of the deformation rate, the strength of the nanoparticles increases, while with increase of the temperature it decreases. For example, with increase of the rate of compression of the particles of the diameter of 10 nm by 100 m/s (within the rate range from 2 to 500 m/s) the strength increased approximately by 8−13 % depending on orientation of compression. With increase of the temperature by 100 K (within the range from 0 to 1000 K), the strength dropped by 3−5 %.

2. When the single-crystal nanoparticles are deformed, there is anisotropy of the mechanical properties. In particular,the compressive strength along the directions [111] and [110] was always noticeably higher than the compressive strength along [112] approximately by 30−40 %.

3. The following stages of deformation of the single-crystal nanoparticles during compression were identified: formation of the flat „islets“ in points of contact with compressing surfaces, cooperative rotation of the entire structure of the particle, formation of dislocations near the „islets“ and their propagation. As the size of the single-crystal particle was reduced, the portion of the structure rotation stage increased.

4. As the size of the nanoparticles (both the single-crystal ones as well as the amorphous ones) is reduced, their strength increased and the value of deformation, at which the maximum stress was achieved, increased, too. At the same time, the strength values for the amorphous particles turned out to be in several times less than those for the single-crystal particles.

5. When the amorphous nanoparticles were compressed, in most cases we observed the phenomenon of compaction and partial crystallization of the structure near the points of load application, which was especially pronounced usually when deformation had the values of more than 8−10 %. With further compression, the particle was usually crystallized completely with formation of the nanocrystalline structure.

Conflict of interest

The authors declare that they have no conflict of interest.

References

[1] Dekker Encyclopedia of Nanoscience and Nanotechnology, 3rd ed. / Eds J.A. Schwarz, S.E. Lyshevski, C.I. Contescu). CRC Press, Boca Raton (2014). 4200 p.

[2] C. Humbert, T. Noblet, L. Dalstein, B. Busson, G. Barbillon. Mater. **12**, *5*, 836 (2019). https://doi.org/10.3390/ma12050836

[3] Y. Mantri, J.V. Jokerst. ACS Nano **14**, *8*, 9408 (2020). https://doi.org/10.1021/acsnano.0c05215

[4] T.K. Jain, M.A. Morales, S.K. Sahoo, D.L. Leslie-Pelecky, V. Labhasetwar. Mol. Pharm. **2**, *3*, 194 (2005). https://doi.org/10.1021/mp0500014

[5] S.-Y. Shim, D.-K. Lim, J.-M. Nam. Nanomedicine **3**, *2*, 215 (2008). https://doi.org/10.2217/17435889.3.2.215

[6] K. Kodama, T. Nagai, A. Kuwaki, R. Jinnouchi, Y. Morimoto. Nature Nanotechnol. **16**, *2*, 140 (2021). https://doi.org/10.1038/s41565-020-00824-w

[7] S. Mitchell, R. Qin, N. Zheng, J. Pérez-Ramirez. Nature Nanotechnol. **16**, *2*, 129 (2021). https://doi.org/10.1038/s41565-020-00799-8

[8] C.E. Carlton, P.J. Ferreira. Micron **43**, *11*, 1134 (2012). https://doi.org/10.1016/j.micron.2012.03.002

[9] J. Deneen, W.M. Mook, A. Minor, W.W. Gerberich, C.B. Carter. J. Mater. Sci. **41**, *14*, 4477 (2006). https://doi.org/10.1007/s10853-006-0085-9

[10] W.W. Gerberich, W.M. Mook, C.R. Perrey, C.B. Carter, M.I. Baskes, R. Mukherjee, A. Gidwani, J. Heberlein, P.H. McMurry, S.L. Girshick. J. Mech. Phys. Solids **51**, *6*, 979 (2003). https://doi.org/10.1016/S0022-5096(03)00018-8

[11] D.D. Stauffer, A. Beaber, A. Wagner, O. Ugurlu, J. Nowak, K.A. Mkhoyan, S. Girshick, W. Gerberich. Acta Materialia **60**, *6–7*, 2471 (2012). https://doi.org/10.1016/j.actamat.2011.10.045

[12] M. Ramos, L. Ortiz-Jordan, A. Hurtado-Macias, S. Flores, J.T. Elizalde-Galindo, C. Rocha, B. Torres, M. Zarei-Chaleshtori, R.R. Chianelli. Mater. **6**, *1*, 198 (2013). https://doi.org/10.3390/ma6010198

[13] A. Sharma, J. Hickman, N. Gazit, E. Rabkin, Y. Mishin. Nature Commun. **9**, *1*, 4102 (2018). https://doi.org/10.1038/s41467-018-06575-6

[14] J. Bian, H. Zhang, X. Niu, G. Wang. Crystals **8**, *3*, 116 (2018). https://doi.org/10.3390/cryst8030116

[15] J.J. Bian, L. Yang, X.R. Niu, G.F. Wang. Phil. Mag. **98**, *20*, 1848 (2018). https://doi.org/10.1080/14786435.2018.1459059

[16] D. Mordehai, S.-W. Lee, B. Backes, D.J. Srolovitz, W.D. Nix, E. Rabkin. Acta Materialia **59**, *13*, 5202 (2011). https://doi.org/10.1016/j.actamat.2011.04.057

[17] W.-Z. Han, L. Huang, S. Ogata, H. Kimizuka, Z.-C. Yang, C. Weinberger, Q.-J. Li, B.-Y. Liu, X.-X. Zhang, J. Li, E. Ma, Z.-W. Shan. Adv. Mater. **27**, *22*, 3385 (2015). https://doi.org/10.1002/adma.201500377

[18] Y. Hong, N. Zhang, M.A. Zaeem. Acta Materialia **145**, 8 (2018). https://doi.org/10.1016/j.actamat.2017.11.034

[19] J. Amodeo, L. Pizzagalli. Comptes Rendus. Physique, Plasticity & Solid State Phys. **22**, *S3*, 35 (2021). https://doi.org/10.5802/crphys.70

[20] Y. Feruz, D. Mordehai. Acta Materialia **103**, 433 (2016). http://dx.doi.org/10.1016/j.actamat.2015.10.027

[21] D. Guo, G. Xie, J. Luo. J. Phys. D Appl. Phys. **47**, *1*, 013001 (2014). https://doi.org/10.1088/0022-3727/47/1/013001

[22] K.A. Krylova, L.R. Safina, R.T. Murzaev, S.A. Shcherbinin, Yu.A. Baimova, R.R. Mulyukov. FTT **65**, *9*, 1579 (2023). https://doi.org/10.21883/FTT.2023.09.56256.101 (in Russian).

[23] K.A. Krylova, L.R. Safina, R.T. Murzaev, J.A. Baimova, R.R. Mulyukov. Mater. **14**, *11*, 3087 (2021). https://doi.org/10.3390/ma14113087

[24] L.R. Safina, J.A. Baimova, R.R. Mulyukov. Mech. Adv. Mater. Mod. Processes **5**, *1*, 2 (2019). https://doi.org/10.1186/s40759-019-0042-3

[25] D. Kiener, A.M. Minor. Nano Lett. **11**, *9*, 3816 (2011). https://doi.org/10.1021/nl201890s

[26] F. Mompiou, M. Legros, A. Sedlmayr, D.S. Gianola, D. Caillard, O. Kraft. Acta Materialia **60**, *3*, 977 (2012). https://doi.org/10.1016/j.actamat.2011.11.005

[27] D.J. Dunstan, A.J. Bushby. Int. J. Plast. **40**, 152 (2013). https://doi.org/10.1016/j.ijplas.2012.08.002

[28] P.S. Phani, K.E. Johanns, E.P. George, G.M. Pharr. Acta Materialia **61**, *7*, 2489 (2013). https://doi.org/10.1016/j.actamat.2013.01.023

[29] D. Kilymis, C. Gerard, L. Pizzagalli. TMS 2019 148th Annual Meeting & Exhibition Supplem. Proceed. The Minerals, Metals & Materials Series, 1347 (2019). https://doi.org/10.1007/978-3-030-05861-6_128

[30] H.K. Issa, A. Taherizadeh, A. Maleki. Ceram. Int. **46**, *13*, 21647 (2020). https://doi.org/10.1016/j.ceramint.2020.05.272

[31] J. Zhao, S. Nagao, G.M. Odegard, Z. Zhang, H. Kristiansen, J. He. Nanoscale Res. Lett. **8**, *1*, 541 (2013). https://doi.org/10.1186/1556-276X-8-541

[32] A.R. Beaber, J.D. Nowak, O. Ugurlu, W.M. Mook, S.L. Girshick, R. Ballarini, W.W. Gerberich. Phil. Mag. **91**, *7–9*, 1179 (2011). https://doi.org/10.1080/14786435.2010.487474

[33] J. Sun, L. He, Y.C. Lo, T. Xu, H. Bi, L. Sun, Z. Zhang, S.X. Mao, J. Li. Nature Mater. **13**, *11*, 1007 (2014). https://doi.org/10.1038/nmat4105

[34] I. Issa, J. Amodeo, J. Réthore, L. Joly-Pottuz, C. Esnouf, J. Morthomas, M. Perez, J. Chevalier, K. Masenelli-Varlot. Acta Materialia **86**, 295 (2015). https://doi.org/10.1016/j.actamat.2014.12.001

[35] W.M. Mook, J.D. Nowak, C.R. Perrey, C.B. Carter, R. Mukherjee, S.L. Girshick, P.H. McMurry, W.W. Gerberich. Phys. Rev. B **75**, *21*, 214112 (2007). https://doi.org/10.1103/PhysRevB.75.214112

[36] W.W. Gerberich, D.D. Stauffer, A.R. Beaber, N.I. Tymiak. J. Mater. Res. **27**, *3*, 552 (2012). https://doi.org/10.1557/jmr.2011.348

[37] S.-X. Liang, L.-C. Zhang, S. Reichenberger, S. Barcikowski. Phys. Chem. Chem. Phys. **23**, *19*, 11121 (2021). https://doi.org/10.1039/D1CP00701G

[38] J. Sun, S.K. Sinha, A. Khammari, M. Picher, M. Terrones, F. Banhart. Carbon **161**, 495 (2020). https://doi.org/10.1016/j.carbon.2020.01.067

[39] Y. Qian, A. da Silva, E. Yu, C.L. Anderson, Y. Liu, W. Theis, P. Ercius, T. Xu. Nature Commun. **12**, *1*, 2767 (2021). https://doi.org/10.1038/s41467-021-22950-2

[40] Y. Pei, G. Zhou, N. Luan, B. Zong, M. Qiao, F. Tao. Chem. Soc. Rev. **41**, *24*, 8140 (2012). https://doi.org/10.1039/c2cs35182j

[41] Z. Jia, Q. Wang, L. Sun, Q. Wang, L.-C. Zhang, G. Wu, J.-H. Luan, Z.-B. Jiao, A. Wang, S.-X. Liang, M. Gu, J. Lu. Adv. Funct. Mater. **29**, *19*, 1807857 (2019). https://doi.org/10.1002/adfm.201807857

[42] Q. Chen, Z. Yan, L. Guo, H. Zhang, L.-C. Zhang, W. Wang. J. Mol. Liq. **318**, 114318 (2020). https://doi.org/10.1016/j.molliq.2020.114318
[43] A.M. Goryaeva, C. Fusco, M. Bugnet, J. Amodeo. Phys. Rev. Mater. **3**, *3*, 033606 (2019). https://doi.org/10.1103/PhysRevMaterials.3.033606
[44] G.P. Purja Pun, Y. Mishin. Phil. Mag. **89**, *34–36*, 3245 (2009). https://doi.org/10.1080/14786430903258184
[45] E.V. Levchenko, T. Ahmed, A.V. Evteev. Acta Materialia **136**, 74 (2017). https://doi.org/10.1016/j.actamat.2017.06.056
[46] G.M. Poletaev, Y.V. Bebikhov, A.S. Semenov, M.D. Starostenkov. Lett. Mater. **11**, *4*, 438 (2021). https://doi.org/10.22226/2410-3535-2021-4-438-441
[47] G.M. Poletaev, D.V. Dmitrienko, V.V. Diabdenkov, V.R. Mikrukov, M.D. Starostenkov. Phys. Solid State **55**, *9*, 1920 (2013). https://doi.org/10.1134/S1063783413090254
[48] G.M. Poletaev, Y.Y. Gafner, S.L. Gafner. Lett. Mater. **13**, *4*, 298 (2023). https://doi.org/10.22226/2410-3535-2023-4-420-425
[49] G.M. Poletaev, Y.V. Bebikhov, A.S. Semenov. Mater. Chem. Phys. **309**, 128358 (2023). https://doi.org/10.1016/j.matchemphys.2023.128358
[50] J.M. Montejano-Carrizales, M.P. Iñiguez, J.A. Alonso. J. Cluster Sci. **5**, *2*, 287 (1994). https://doi.org/10.1007/BF01170713
[51] F. Baletto, R. Ferrando, A. Fortunelli, F. Montalenti, C. Mottet. J. Chem. Phys. **116**, *9*, 3856 (2002). https://doi.org/10.1063/1.1448484
[52] A. Tilocca. J. Chem. Phys. **139**, *11*, 114501 (2013). https://doi.org/10.1063/1.4821150
[53] A.D. Evstifeev, A.A. Gruzdkov, Y.V. Petrov. Tech. Phys. **58**, *7*, 989 (2013). https://doi.org/10.1134/S1063784213070086

Translated by M.Shevelev